JOURNAL OF MATERIALS SCIENCE **34** (1999) 5605–5612

Effect of AlN and Al_2O_3 additions on the phase relationships and morphology of SiC

Part I *Compositions and properties*

GREG E. HILMAS
Department of Ceramic Engineering, University of Missouri-Rolla, Rolla, MO 65409-0330
E-mail: ghilmas@umr.edu

TSENG-YING TIEN
Department of Materials Science and Engineering, The University of Michigan, Ann Arbor, MI 48109-2136

X-ray diffraction was utilized to follow the transformation from β-SiC (3C) to the various α-SiC polytypes in the presence of AlN and Al_2O_3 additives after hot pressing from 1700 to 2100 °C. The 2H- and 6H-polytypes of α-SiC were the predominate polytypes with additions of only AlN or Al_2O_3, respectively. The amount of 2H- and 6H-polytypes, and subsequently the microstructural morphology of the SiC materials, were found to be controlled by varying the amount of AlN and Al_2O_3. Improvements in fracture toughness to ~9 MPa-$\sqrt{m}$ were achieved with flexural strengths ranging from 600 to 900 MPa. These results suggest that accurate control of the polytypic make-up of SiC-based materials, along with their mechanical properties, can be achieved through AlN and Al_2O_3 additions.

1. Introduction

The transformation of β-SiC (3C) at high temperature to one or more of the α-SiC polytypes (2H, 4H, 15R, 6H, etc.) has been investigated extensively with results showing the transformation and the resulting α-polytype formed to be strongly dependent on the polytypic make-up of the starting SiC powder, the sintering temperature, and the amount and type of additives used [1, 2]. Small additions of Al, B, and C or BeO to β-SiC (3C) have predominantly resulted in transformation to the 4H-polytype of α-SiC [3]. While small additions of only B and C to β-SiC have produced transformations to the 6H-polytype [4]. Strongly affected by the present research is the finding by several authors that β-SiC (3C) preferentially transforms to α-SiC (2H) in the presence of AlN (2H). This can occur over a broad range of SiC-AlN mixtures, typically from 35 to 100 wt % AlN, and is accompanied by an extensive 2H solid-solution above 2050 °C [5, 6].

The intent of this study was to control the overall phase content, microstructural morphology and mechanical properties of a series of SiC-based composites utilizing both AlN and Al_2O_3 as additives. This paper will deal mainly with the processing, fabrication, post-fabrication phase analysis, and mechanical properties of the compositions. Emphasis is on observing the transformation from β-SiC to one or more of the α-SiC polytypes and determination of the phase content in terms of percent SiC-polytypes. Mechanical properties results include measurements of the room temperature fracture toughness, and flexural strengths at both room temperature and elevated temperatures.

The second paper will describe in detail the morphology of the microstructures formed in this series of compositions and will show that the major SiC-polytype formed and its resultant morphology are strongly affected by the quantity of AlN and Al_2O_3 added to the starting SiC powder.

2. Experimental procedure

2.1. Compositions and powder processing

The ceramic raw materials used in this study were SiC, AlN and Al_2O_3. The starting SiC powder was β-SiC (Grade B10, >95% β-SiC (3C), Hermann C. Starck, Goslar, FRG) with a mean particle size of 0.6 μm. The major impurities in the SiC powder are 0.92% O, 0.024% Fe and 0.011% Al. The AlN powder (Keramont Corp., Tucson, AZ) had an average particle size $\leq$1.0 μm and the major impurities were 1.2% O and 0.2% C. The Al_2O_3 (Grade A-16, Alcoa Industrial Chemicals, Bauxite, AR) had an average particle size 0.7 μm and the major impurities were 0.006% Fe.

The compositions formed are outlined in Table I and are referred to by their respective starting powders in terms of volume percent of β-SiC powder with a 3 : 1 molar ratio of $AlN : Al_2O_3$ making up the remainder of each composition: i.e. 90 vol % β-SiC + 10 vol % $3AlN : 1Al_2O_3$ = BS90. Each composition also contained 0.5 wt % B added as a sintering aid. The 3 : 1

TABLE I Compositions of β-SiC : AlN : Al_2O_3 series and standards

	Vol %		wt %		
Sample	β-SiC	3AlN : 1Al_2O_3	SiC	AlN	Al_2O_3
BS50	50	50	47.55	28.67	23.78
BS60	60	40	57.62	23.17	19.21
BS70	70	30	67.91	17.54	14.55
BS80	80	20	78.39	11.81	9.80
BS90	90	10	89.08	5.97	4.95
BS100	100	—	100	—	—
BS90 : 10N	90	10 AlN	89.88	10.12	—
BS90 : 10O	90	10 Al_2O_3	87.94	—	12.06

molar ratio for the AlN : Al_2O_3 additions was chosen through extensive research by the authors in an attempt to form several AlN-polytypoids [7] ($Al_5O_2N_3$ for the 3 : 1 composition) *in situ* within a SiC matrix [8]. Early results showed that SiC compositions hot-pressed above 2050 °C, and containing 20 weight percent of the 3 : 1 AlN : Al_2O_3 molar additions, achieved near theoretical density with a fracture toughness nearly twice that of phase pure SiC processed under the same conditions. The current paper is an expansion of these results whereby the additions of 3AlN : 1Al_2O_3 are being varied with respect to the SiC matrix material.

The compositions were prepared by attrition milling raw powders as 50 g charges in a teflon lined milling jar using 2 mm diameter alumino-silicate milling media and isopropyl alcohol. The milling time was 3 h for each composition. The milled slurry was then oven dried overnight at 85 °C to obtain the powder.

2.2. Specimen fabrication

In preparation for hot-pressing, the milled and dried powder was placed in a graphite die that was lightly coated with boron nitride powder to suppress bonding of the SiC to the die during hot-pressing. The powder was cold-pressed uniaxially in the die under a 25 MPa load and then placed in a graphite resistance furnace, and heated under vacuum to 1000 °C at a rate of approximately 40 °C/min. At 1000 °C the furnace was flushed and filled with nitrogen gas, and the heating rate was increased to approximately 60°/min. A 'flowing' nitrogen atmosphere of slightly greater than 1 atm was constantly maintained in attempt to limit decomposition of the phases at high temperature. A 25 MPa load was applied during the heating cycle above 1000 °C and released upon cooling below 1000 °C. The compositions (BS90, BS80, BS70, BS60 and BS50) were prepared by hot-pressing at 1700, 1800, 1900, and 2000 °C for 1 h hold times and at 2100 °C for times of 1, 2 and 5 h. All specimens hot-pressed at 1800 °C and above were >98% dense as measured by water displacement.

In order to determine the effect of the AlN and Al_2O_3 additives on the polytypic phase content of the SiC matrix, three standards were also prepared by hot pressing at 2100 °C for 1 h using the processing method described above. These standards included 100% β-SiC (BS100), 90 vol % β-SiC with 10 vol % AlN (BS90 : 10N), and 90 vol % β-SiC with 10 vol % Al_2O_3(BS90 : 10O).

2.3. X-ray diffraction analysis

Often overlooked in the study of SiC is the difficulty in readily determining the overall SiC-polytype phase content from bulk analytical methods like X-ray diffraction. The multitude of possible transformations, the presence of many of the polytypes during high temperature forming, and ultimately the overlap of their diffraction peaks makes quantification difficult. The accepted method to accomplish this goal has been to utilize the experimentally calculated and measured single-crystal data, and thus quantified X-ray intensity equations of Ruska *et al*. [9]. Unfortunately, their results do not allow for the presence of the 2H-polytype of α-SiC which is present in our material. However, the calculations are relatively straightforward, permitting the 2H-polytype to be added to their results [8]. In brief, the atomic positions for the 2H-polytype (space group—$P6_3mc$) were obtained from Wyckoff [10]. In line with the calculations of Ruska *et al.* [9], atomic scattering factors were calculated using Si^{2+} and C^{2-} calculated by linear extrapolation from tabulated data [11] for Si^0, Si^{3+} and C^0, C^{2+}. The X-ray intensities were then calculated from the following equation:

$$I_n = m[F]^2 \times \mathrm{LP}/V^2$$

where I_n is the intensity normalized to the unit cell volume-V, m is the multiplicity, F is the structure factor, and LP is the Lorentz-polarization factor. Table II shows the factors and resultant X-ray intensities for the 2H-polytype for the reflections in the range of 0.266 to 0.217 nm. These intensities were then normalized to the strongest diffraction line or I_{100} for pure 3C-SiC. Table III outlines the final equations for quantifying the amount of SiC-polytypes utilizing the new calculated data for 2H-SiC and the calculated and measured data for 15R, 6H, 4H and 3C [9].

In order to gain insight into the formation of the different SiC polytypes it was necessary to follow the solid-state transformation among the polytypes during the hot-pressing cycle. Therefore, samples were taken at each temperature and composition from the hot-pressed billets. The samples were then machined into 3 × 3 × 10 mm bars, cleaned, and crushed into a fine powder using a vibratory tungsten carbide ball and mortar. The powder samples were evaluated by X-ray diffraction (XRD) performed on a rotating anode diffractometer* utilizing monochromated CuK_α radiation. A 60 rpm motor was added to the X-ray stage to rotate the samples. Along with using a fine powder, the rotation of the sample helps to eliminate any disparity between calculated and observed X-ray intensities due to both extinction and preferred orientation. The range scanned was 32° to 45° 2θ, and the low rpm motor required scan rates to be slowed to 1°/min.

* Rigaku/USA, Inc., Model No. RU-200BH, Danvers, MA.

TABLE II Calculated X-ray intensities for the 2H-polytype of α-SiC

h k l	*d* (nm)	*F*	(*F*/*V*)	*m*	LP	I_n
1 0 0	0.2669	14.21	0.3436	6	21.20	15.016
0 0 2	0.2515	20.88	0.5049	6	18.56	9.461
1 0 1	0.2357	12.38	0.2993	12	16.00	17.204

TABLE III Equations for calculating SiC-polytypes from XRD peak intensities

15R[a]		6H[a]		4H[a]		2H		3C[a]		Peak	*d* (nm)
3.2a			+	9.9c	+	39.4d			=	A	0.266
11.2a	+	19.4b							=	B	0.263
26.0a			+	38.9c					=	C	0.257
31.1a	+	59.2b	+	25.1c	+	24.8d	+	100.0e	=	D	0.251
		18.1b	+	34.1c	+	45.1d			=	E	0.235
2.4a	+	6.5b					+	13.1e	=	F	0.217

[a]Calculated and measured data taken from reference [7].

2.4. Mechanical property measurements

Sections of the hot-pressed samples were diamond machined and then ground and polished to a 0.1 μm diamond finish in order to measure microhardness and fracture toughness. A standard Vicker's diamond indenter was placed in a microhardness testing machine* for all measurements. Indentation loads varied from 5 to 25 kg depending upon the sample and to fulfill the requirement that the radial/median cracks be equal to or greater than twice the Vicker's indentation diagonal. The fracture toughness, K_{Ic}, was then calculated from an average of ten indents using the equation of Anstis *et al.* [12].

Flexural strengths and additional fracture toughness measurements were made using four-point bend test techniques [13, 14]. The test bars for four-point bending were diamond machined from each hot-pressed billet to a final size of $20 \times 3 \times 2.25$ mm. In order to alleviate any strength or toughness anisotropy, all test specimens were machined such that the tensile face was perpendicular to the hot-pressing direction. The tensile surfaces were polished to a 1 μm diamond finish, and the edges of the bars were chamfered. All tests were performed using a specially designed self-aligning four-point bend test fixture made from hot-pressed SiC. The fixture also contained cylindrical SiC supports and had an outer span of 16 mm and inner span of 8 mm. A universal Instron testing machine was utilized to fracture the test bars using computer control. The room temperature was ~27 °C, and the crosshead speed, *s*, was 5×10^{-3} in/min. This crosshead speed corresponded to a strain rate, $\dot{\varepsilon}$, of 1×10^{-4}/s. Measurements of the flexural strength, σ, were obtained from three bars at each of four different temperatures (room temperature −27 °C, 900 °C, 1200 °C and 1400 °C).

Fracture toughness in four-point bending was measured by the controlled surface flaw method on BS90 samples to corroborate the data obtained by the indentation technique. A Vicker's diamond indentation was made at the center of the test bars on the tensile surface while making sure to keep the indent oriented orthogonally to the longitudinal axis of the test bar. An indentation load of 15 kg was used for all test bars, and following fracture, K_{Ic} was calculated using the equation of Chantikul *et al.* [15].

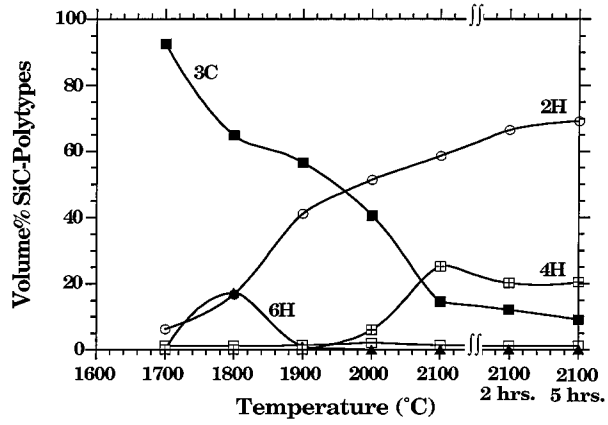

Figure 1 Plot of vol % SiC polytype vs. hot-pressing temperature for composition BS50 hot pressed for 1 h hold times up to 2100 °C, and 2100 °C for 2 and 5 h.

3. Results and discussion

3.1. X-ray diffraction analysis

The data for the BS series samples is shown graphically in Figs 1–5. For each composition, a plot of vol % SiC-polytype versus hot-pressing temperature from 1700 to 2100 °C for hot pressing hold times of 1 h are represented along with data at 2100 °C for hold times of 2 and 5 h. The data clearly shows that the transformation to the high temperature SiC-polytype is compositionally dependent.

Compositions BS50 and BS60 both transform rapidly to the 2H-polytype of SiC, as shown in Figs 1 and 2, respectively. These compositions exhibit an intermediate development of a 6H-polytype with a maximum occurring at 2000 °C for BS60 and 1800 °C for BS50. The 6H-polytype is subsequently consumed at higher temperatures to form more of the 2H-polytype. Appreciable amounts of the 4H-polytype are starting to form along with 2H above 2000 °C, only to be

* Zwick of America, Inc., Model No. 3212, East Windsor, CT.

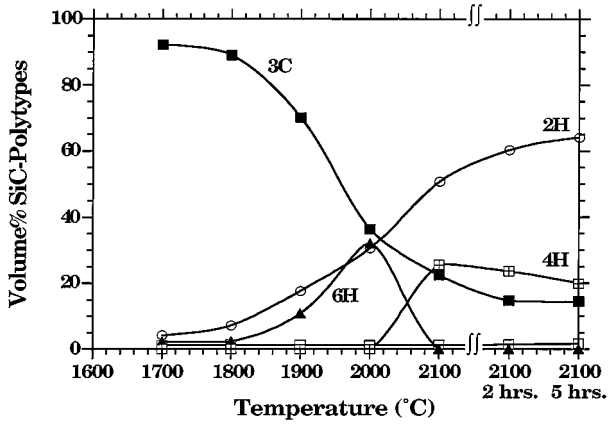

Figure 2 Plot of vol % SiC polytype vs. hot-pressing temperature for composition BS60 hot pressed for 1 h hold times up to 2100 °C, and 2100 °C for 2 and 5 h.

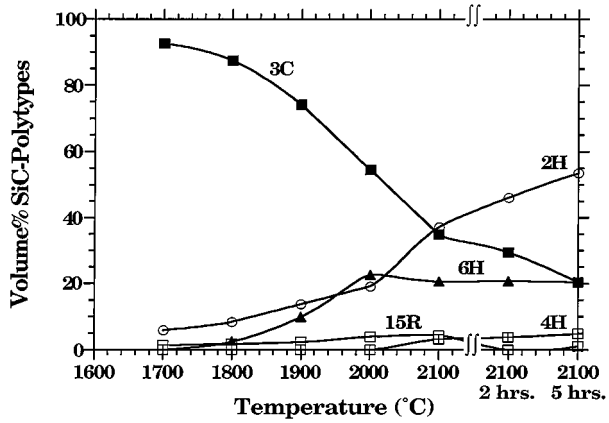

Figure 3 Plot of vol % SiC polytype vs. hot-pressing temperature for composition BS70 hot pressed for 1 h hold times up to 2100 °C, and 2100 °C for 2 and 5 h.

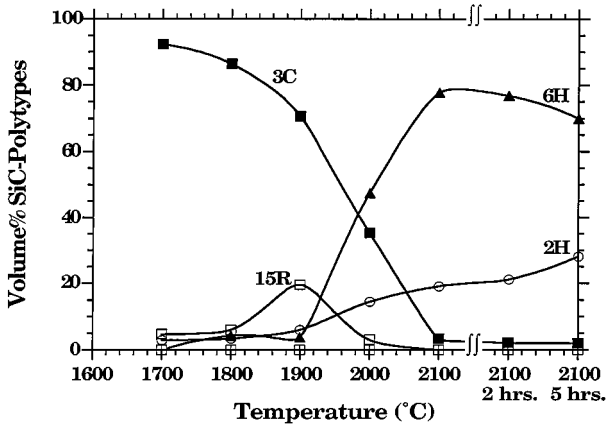

Figure 4 Plot of vol % SiC polytype vs. hot-pressing temperature for composition BS80 hot pressed for 1 h hold times up to 2100 °C, and 2100 °C for 2 and 5 h.

slowly consumed along with more 3C-SiC to form the 2H-polytype. After 5 h at 2100 °C, BS50 and BS60 contain approximately 70 and 65 vol % of 2H-SiC, respectively, 20 vol % of the 4H-polytype, and the remainder being untransformed β-SiC.

The BS70 composition, Fig. 3, shows a strong competition between forming the 2H- and 6H-polytypes. These polytypes start to form slowly above 1800 °C with the 6H-polytype reaching a peak of ~20 vol % at 2000 °C. Only minor quantities of the 4H- and 15R-polytypes form as intermediate phases, never achieving more than 5 vol % of either polytype. While the sample still retains some 3C-SiC after 5 h at 2100 °C, only the 2H-polytype is increasing quantity vs. all other polytypes for times longer than 1 h at 2100 °C.

In Fig. 4, the BS80 composition has transformed predominantly to the 6H-polytype, but with an intermediate development of the 15R-polytype which achieved a maximum of ~20 vol % at 1900 °C. The 15R-polytype was subsequently consumed above 1900 °C in favor of the 6H-polytype and some formation of the 2H-polytype. The quantity of 6H-polytype actually decreased slightly for longer times at 2100 °C. After 5 h at 2100 °C the sample contains 70 vol % of 6H-SiC and ≤30 vol % of 2H-SiC.

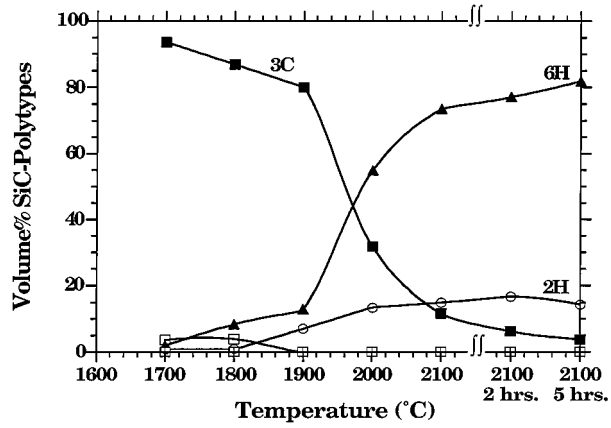

Figure 5 Plot of vol % SiC polytype vs. hot-pressing temperature for composition BS90 hot pressed for 1 h hold times up to 2100 °C, and 2100 °C for 2 and 5 h.

Fig. 5 shows composition BS90 transforming almost exclusively to the 6H-polytype in the range of 1900–2100 °C with only slight amounts of the 2H-polytype. The 2H-polytype forms progressively above 1800 °C, leveling off to ~15 vol % after 5 h at 2100 °C. The final composition contains >80 vol % of 6H-SiC with ~5 vol % of untransformed β-SiC.

The results of this investigation emphasize the composition and additive dependence to the polytypism in the transformed α-SiC matrix. For compositions BS90 and BS80, having 10–20 vol % 3AlN : 1Al_2O_3, respectively, the preferred SiC-polytype is 6H. Larger additions of 30–50 vol % 3AlN : 1Al_2O_3 resulted in a competition between the development of the 6H- and the 2H-polytype, with the 2H-polytype predominating at higher temperatures, longer times, and an increasing percentage of AlN and Al_2O_3 additives. Based on the XRD results after 5 h at 2100 °C, it is apparent that regions of stability exist for the α-SiC polytypes formed under the conditions of this study. The current results are not an attempt to determine the actual 'equilibrium' phase diagram for the SiC-AlN-Al_2O_3 system, but the data does provide a guideline that can be used to exert control over the phase content and microstructural morphology of SiC-based ceramic materials utilizing simultaneous additions of AlN and Al_2O_3.

The XRD data for the standards BS100, BS90 : 10N, and BS90 : 10O is shown in Table IV, including the

major and minor polytypes of SiC that have formed after 1 h at 2100 °C. As expected from previous research [5, 6], the addition of AlN resulted in a transformation to the 2H-polytype of α-SiC. Alternately, additions of Al_2O_3 resulted in a transformation to predominantly the 6H-polytype of α-SiC. The BS100 composition transformed to a mixture of the 6H- and 4H-polytypes of α-SiC along with minor quantities of the 15R- and 3C-polytypes.

TABLE IV X-ray diffraction results for SiC standards

Sample code	Major SiC-polytypes	Minor SiC-polytypes
BS90 : 10N	$2H_{s.s.}$	3C
BS90 : 10O	6H	4H and 3C
BS100	6H and 4H	15R and 3C

TABLE V Mechanical properties of β-SiC : AlN : Al_2O_3 series

Sample[a]	ν	E (GPa)	H (GPa)	K_{Ic} (MPa-$\sqrt{m}$)
β-SiC (Standard)[b]	0.18	437	22.8 ± 0.7	2.7 ± 0.2
BS50	0.19	368	20.3 ± 0.8	2.7 ± 0.2
BS60	0.19	394	21.6 ± 0.6	2.9 ± 0.2
BS70	0.18	406	20.7 ± 0.6	2.8 ± 0.1
BS80	0.19	403	18.6 ± 0.5	5.3 ± 0.3
BS90	0.18	428	14.8 ± 1.0	8.5 ± 0.6

[a]All samples contain 0.5 wt % B added as a sintering aid. [b]Hot-pressed at 2050 °C with 1 wt % B and 1 wt % C added as sintering aids.

3.2. Mechanical property measurements

The results of elastic modulus, Poisson's ratio, hardness, and fracture toughness measurements for samples hot pressed at 2100 °C for 1 h are summarized in Table V. The most prominent results from this data are the fracture toughness and hardness values. The β-SiC standard is typical of hot-pressed SiC materials, having an indentation fracture toughness in the range of 2.5–3.0 MPa-$\sqrt{m}$. Samples BS50, BS60 and BS70 had similar fracture toughness values ranging from 2.7 to 2.9 MPa-$\sqrt{m}$. Sample BS80 showed a definite increase in fracture toughness to 5.3 MPa-$\sqrt{m}$, while the BS90 composition exhibited the greatest increase in fracture toughness, achieving 8.5 MPa-$\sqrt{m}$. Concurrent with the increase in fracture toughness for the latter two compositions is a precipitous decrease in hardness dropping to 18.6 GPa for the BS80 composition to a low of 14.8 GPa for BS90. This combination of properties would most likely be attributed to the formation of microcracks. Although microcracks were not observed in the present work, liquid phase sintered SiC materials have been shown to exhibit microcrack toughening behavior with cracks appearing between SiC grains during crack propagation [16].

Scanning electron microscopy was performed on sample BS90 to try and determine a cause for this drastic increase in fracture toughness. Upon observation of Vicker's indentation produced radial/median cracks in the SEM, coupled with the XRD results, it was apparent that the β-SiC (3C) matrix had transformed into an elongated platelet containing α-SiC (6H) matrix. This microstructure resulted in a strong increase in crack deflection with definite bridging zones left behind the

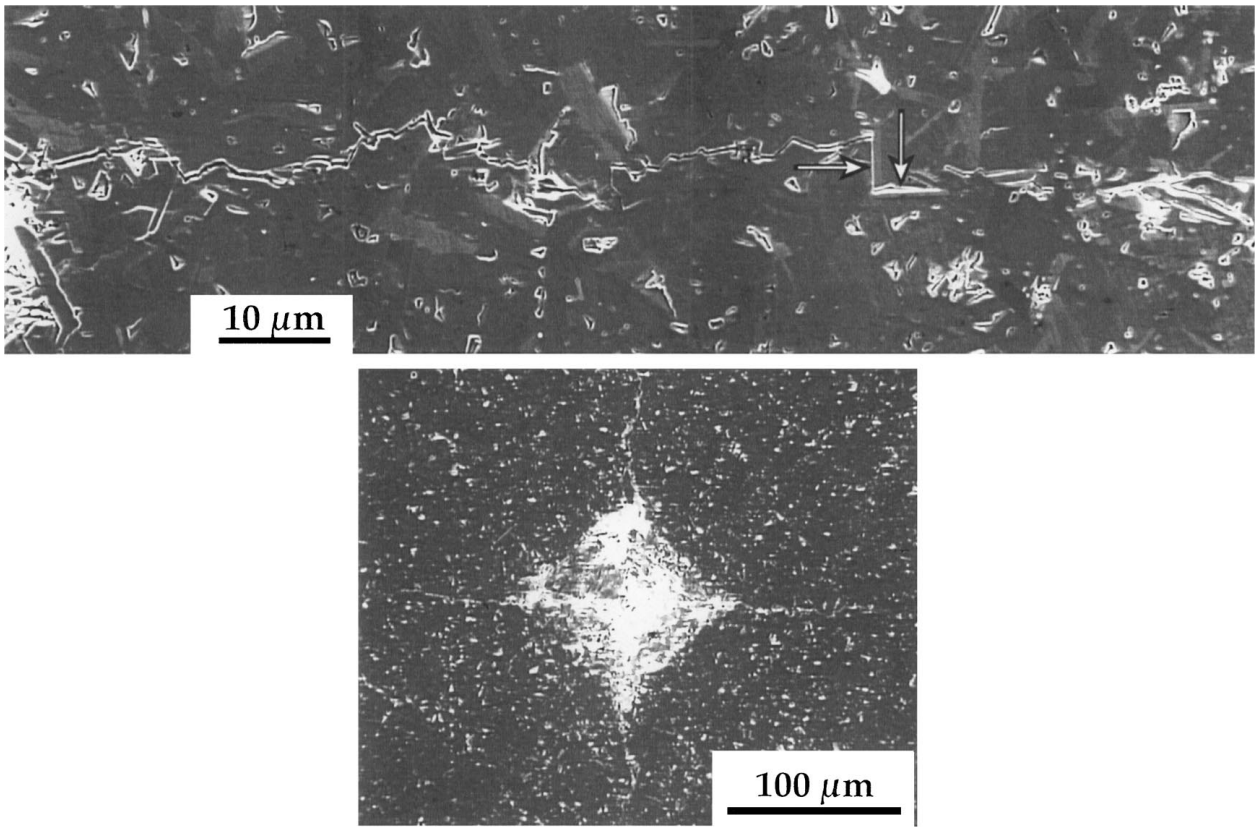

Figure 6 Radial/median cracks produced by a 20 kg Vicker's indent in composition BS90.

advancing crack front. Previous researchers have observed limited to no improvement in the room temperature fracture toughness with the development of an elongated SiC matrix [17–19]. They typically reported that cracks still passed through a majority of the elongated SiC grains resulting in a mostly transgranular mode of brittle fracture. Fig. 6, from samples of the BS90 composition, clearly shows that the radial/median cracks preferred not to pass through the 6H-SiC grains, but to follow a mode of intergranular fracture. The two arrows (inset in the figure) indicate where a radial/median crack has progressed straight into two different 6H-SiC grains. Instead of penetrating the grains, the crack was deflected along the long axis of their interface before continuing on in the direction normal to the applied stress. This type of fracture mode is indicative of 'crack deflection' models [20, 21] showing large increases in fracture toughness with high aspect ratio grains along with weak grain interfaces possibly due to residual tensile stresses at the grain boundaries.

It seems evident from the lack of crack deflection in previous SiC research containing elongated SiC grains [17–19], simply having high aspect ratio grains, either rod-like or platelet-like, was not enough to improve the fracture toughness of those particular compositions. Microstructural development must include control of the interfacial properties contiguous with design of the morphology of the microstructure to give rise to an improved toughening effect. This can occur through changes in the bonding strength and/or interfacial stress state between the matrix grains themselves or between the matrix and a dispersed second phase.

Methods for varying the interfacial stress state have typically included the addition of dispersed particulates or whisker reinforcements [22–25] and/or the addition of an intergranular phase [26, 27]. Assuming that the intergranular phase forms a continuous layer throughout the matrix, and its thermal expansion coefficient is significantly different than that of the matrix, a high stress state can be created at the interface. Additionally, if the thermal expansion coefficient of the intergranular phase is greater than that of the matrix, during cooling from the processing temperature, a 'tensile' stress state will develop at the interface. This leads to a reduced bond strength and even microcracking at the interface if the thermal expansion coefficient of the intergranular phase is significantly high. Reduced bonding at the interface should result in improved fracture toughness for both ceramic monoliths and composites.

Crack deflection processes have also been shown to be enhanced by several other microstructural effects. The fracture path of an advancing crack has been shown to be altered by impurities at the grain boundaries and multi-grain junctions [28, 29], residual grain boundary porosity due to incomplete densification or poor processing [30], and residual tensile strains at the grain boundaries due to thermal expansion anisotropies in single phase polycrystalline materials [31]. An overview of toughening effects due to crack deflection, crack bridging and pullout including the effects of grain size and platelet formation, along with the effects of intergranular phases and stress induced microcracking has been written by Becher [32].

In the present study, no concerted effort was made to manipulate the interfacial stress state through the addition of an intergranular phase. Nevertheless, the improvements in fracture toughness are fundamental to the BS80 and BS90 compositions. From the above considerations of toughening enhancements, the increases observed in these materials are most likely produced by substantial residual tensile stresses at the grain boundaries possibly even giving rise to interfacial microcracking during crack propagation. The tensile stress state may have been affected both by the presence of an intergranular oxide phase and by stresses produced due to the thermal expansion and elastic modulus anisotropy associated with the large α-SiC (6H) grains which have grown rapidly following the SiC phase transformation. Li and Bradt [33] have shown that the anisotropic behavior of SiC can lead to substantial thermoelastic stresses during cooling. This is most pronounced in the BS80 and BS90 compositions, and a strong case for microcracking is corroborated by their decrease in hardness concurrent with increasing fracture toughness.

In addition to the fracture toughness measurements obtained by the 'Direct Crack Measurements' technique [12], fracture toughness data was also obtained on three BS90 samples using the 'Controlled Surface Flaw' technique [15]. The fracture toughness values, summarized in Table VI, were uniform and had an average of 8.9 ± 0.4 MPa-$\sqrt{\text{m}}$. This was comparable to the direct crack measurement data obtained earlier, included in Table VI, where a fracture toughness value of $\sim 8.5 \pm 0.6$ MPa-$\sqrt{\text{m}}$ was obtained.

The high fracture toughness values obtained for the BS90 samples were emphasized by the large crack deflections as suggested by the observation of radial/median cracks produced by Vicker's indents (Fig. 6). The cracks are seen to deflect out of the plane normal to the applied stress. They follow a tortuous intergranular path through the microstructure to avoid the platelet shaped SiC grains.

Fracture toughness measurements were also performed on all samples hot pressed for 2 and 5 h at 2100 °C. The data is shown in Fig. 7 along with the data obtained at 2100 °C for a 1 h hold time. The change in

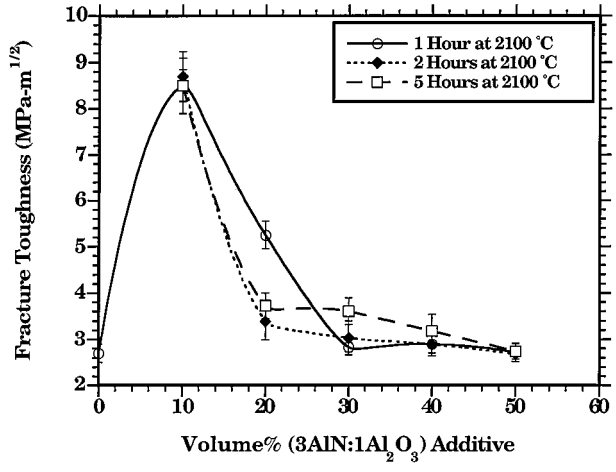

Figure 7 Fracture toughness vs. vol % additive for β-SiC : AlN : Al_2O_3 series hot pressed at 2100 °C for 1, 2, and 5 h.

TABLE VI Mechanical property data for BS90 composites hot-pressed for 1 h at 2100 °C

Sample	Width (mm)	Thickness (mm)	E (GPa)	H (GPa)	K_{Ic} (CSF)[a] (MPa-$\sqrt{m}$)	K_{Ic} (DCM)[b] (MPa-$\sqrt{m}$)
BS90-4	3.04	2.25	428	14.7	8.4	—
BS90-5	3.04	2.25	428	14.7	9.2	—
BS90-9	3.04	2.25	428	14.7	9.0	—
BS90	—	—	428	14.7	—	8.5 ± 0.6

[a]CSF: Controlled surface flaw measurement. [b]DCM: Direct radial/median crack measurement.

the fracture toughness values for compositions BS90, BS60, and BS50 for the longer hot pressing times was insignificant, while the fracture toughness of composition BS80 decreased and BS70 increased slightly. Again, XRD showed that the latter two compositions had not reached equilibrium after 1 h at 2100 °C, and therefore showed marked changes in polytypic phase content between 1 and 5 h at 2100 °C (Figs 4 and 3, respectively).

3.3. Flexural strength

The results of the flexural strength measurements are summarized separately for each composition in Figs 8–10. The flexural strength values were quite consistent, denoting a narrow flaw size distribution as indicated by the small error bars in the figures. The BS50 composition exhibited room temperature flexural strength values of 825–900 MPa. These values fell off gradually with increasing temperature to 1400 °C achieving strengths ≤500 MPa. Increasing the hot pressing hold time at 2100 °C, a 5–10% gain in strength for all test temperatures. The BS60 composition is similar in strength to the BS50 composition except at room temperature. The room temperature strength after 1 and 2 h at 2100 °C was ∼650 MPa but increased to >800 MPa after 5 h at 2100 °C. The room temperature strengths of composition BS70 were in the range of 750–825 MPa. The strength level for both the BS60 and BS70 compositions decreased significantly with increasing temperature to a low of ∼400 MPa at 1400 °C. Since these three compositions were quite similar in their overall flexure behavior, their data has been summarized in Fig. 8 as a plot of flexural strength as a function of temperature for the longest hot pressing hold time of 5 h at 2100 °C.

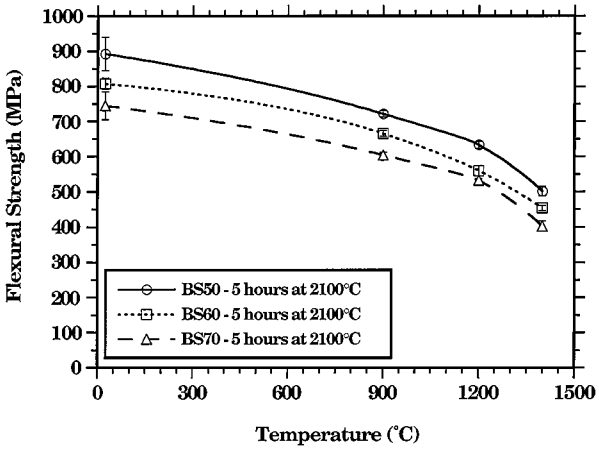

Figure 8 Plot of flexural strength vs. temperature for compositions BS50, BS60, and BS70 hot pressed for 5 h at 2100 °C.

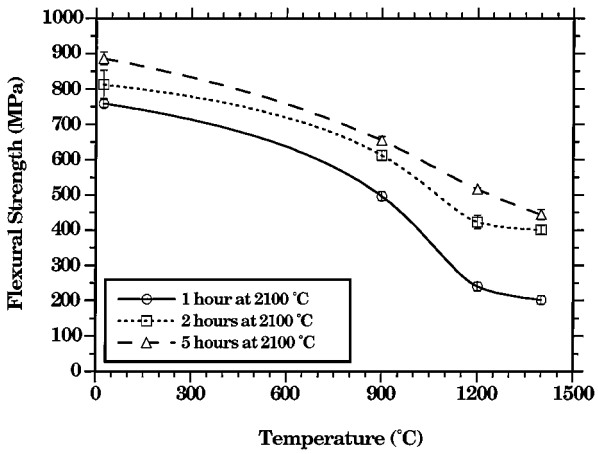

Figure 9 Plot of flexural strength vs. temperature for composition BS80 hot pressed for times of 1, 2, and 5 h at 2100 °C.

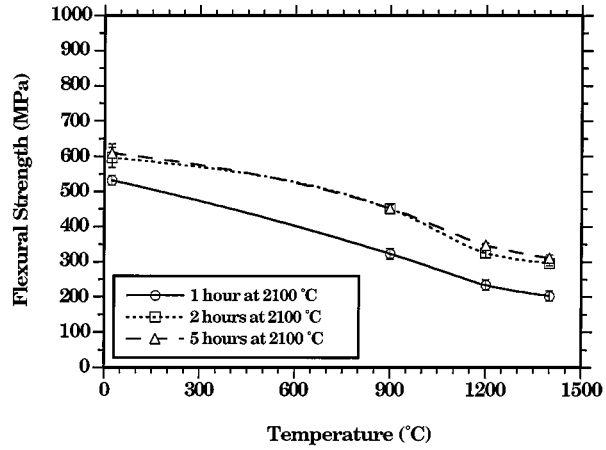

Figure 10 Plot of flexural strength vs. temperature for composition BS90 hot pressed for times of 1, 2, and 5 h at 2100 °C.

The BS80 composition, shown in Fig. 9, exhibited marked changes in flexural strength with both bend test temperature and hot pressing time. The room temperature strength increased from >750 MPa after 1 h at 2100 °C to >875 MPa after 5 h. BS80 samples hot pressed only 1 h at 2100 °C decreased in strength fairly rapidly above 900 °C to a low of 200 MPa, but those hot pressed for 5 h at 2100 °C decreased in strength gradually to a strength of ∼450 MPa.

The BS90 composition, shown in Fig. 10, had the lowest room temperature strength values of all five compositions, although was still high for a SiC composite,

ranging from 525 to 600 MPa. The strength values were consistently 100 MPa higher for longer hot pressing times of 2 and 5 h, while decreasing gradually at higher bend test temperatures. The highest strengths were $\geq$300 MPa at 1400 °C.

4. Conclusions

XRD results showed that the polytypic content of a SiC matrix phase after hot pressing for 5 h at 2100 °C is strongly affected by the amount of AlN and Al_2O_3 additions, with the two most predominate polytypes of α-SiC being 2H and 6H. Additions of only AlN resulted in a preferred transformation from β-SiC to the 2H-polytype of α-SiC, while additions of only Al_2O_3 resulted in transformation to the 6H-polytype of α-SiC.

Mechanical property data showed significant improvements in fracture toughness over hot pressed β-SiC (standard) materials. Fracture toughness values near 9 MPa-$\sqrt{m}$ were achieved for samples of nominal composition 90 vol % SiC : 10 vol % ($3AlN : 1Al_2O_3$). Improvements in the fracture toughness appear to be the result of deflection of the cracks around elongated platelet-like SiC grains in an intergranular mode of fracture. Accompanying the improvements in fracture toughness were a notable decrease in hardness suggesting that microcracking may be responsible for the observed properties. For larger additions of AlN and Al_2O_3 (i.e. >30 vol % $3AlN : 1Al_2O_3$), the fracture toughness values were <3 MPa-$\sqrt{m}$ and comparable to conventional SiC materials.

The entire series of $SiC : AlN : Al_2O_3$ composites exhibited high flexural strengths, with values ranging from 600 MPa to nearly 900 MPa at room temperature. The flexural strengths decreased gradually with increasing four-point bend test temperature for all of the compositions, typically to values that were ~50% of the room temperature value at 1400 °C.

Acknowledgement

This work was supported by the US Department of Energy, Office of Transportation Technologies, Advanced Materials Development Program under Contract No. DE-AC05-84OR2140.

References

1. S. SHINOZAKI and K. R. KINSMAN, in Proc. of the 14th Univ. Conf. on Ceramic Science of Processing of Crystalline Ceramics, edited by H. Palmer, R. F. Davis and T. M. Hare (North Carolina State Univ., Raleigh, NC, 1977) pp. 641–652.
2. Y. TAJIMA and W. D. KINGERY, *J. Amer. Ceram. Soc.* **65**(2) (1982) C27–C29.
3. S. S. SHINOZAKI, J. HANGAS, K. MAEDA and A. SOETA, in "Ceramic Transactions," Vol. 2, Silicon Carbide '87, edited by J. D. Cawley and C. E. Semler (The American Ceramic Society, Westerville, OH, 1989) pp. 113–121.
4. R. M. WILLIAMS, B. N. JUTERBOCK, C. R. PETERS and T. J. WHALEN, *J. Amer. Ceram. Soc.* **67**(4) (1984) C62–C64.
5. R. RUH and A. ZANGVIL, *ibid.* **65**(5) (1982) 260–65.
6. W. RAFANIELLO, PhD dissertation, The University of Utah, June, 1984.
7. L. J. GAUCKLER, H. L. LUKAS and G. PETZOW, *J. Amer. Ceram. Soc.* **58**(7) (1975) 346–47.
8. G. E. HILMAS, PhD dissertation, The University of Michigan, April, 1993.
9. J. RUSKA, L. J. GAUCKLER, J. LORENZ and H. U. REXER, *J. Mat. Sci.* **14** (1979) 2013–2017.
10. R. WYCKOFF, in "Crystal Structures," Vol. 1, 2nd ed. (Interscience, New York, 1963).
11. C. H. MACGILLAVRY and G. D. RIECK (eds.), "International Tables for X-ray Crystallography," Vol. 3 (Kynmoch Press, Birmingham, 1962).
12. G. R. ANSTIS, P. CHANTIKUL, B. R. LAWN and D. B. MARSHALL, *J. Amer. Ceram. Soc.* **64**(9) (1981) 533–538.
13. Proposed MIL-STD-1942A, "Flexure Strength of High Performance Ceramics at Ambient Temperatures," US Army Materials Technology Laboratory, Watertown, MA, 1990.
14. Y. MURAKAMI (ed.), "Stress Intensity Factors Handbook," (Pergamon Press, New York, 1987).
15. P. CHANTIKUL, G. R. ANSTIS, B. R. LAWN and D. B. MARSHALL, *J. Amer. Ceram. Soc.* **64**(9) (1981) 539–543.
16. H.-J. KLEEBE, *J. Eur. Ceram. Soc.* **10** (1992) 151–159.
17. G. ORANGE, H. TANAKA and G. FANTOZZI *Ceram. Int.* **13** (1987) 159–165.
18. S. G. SESHADRI, M. SRINIVASAN and K. Y. CHIA, in "Ceramic Transactions," Vol. 2, Silicon Carbide '87, edited by J. D. Cawley and C. E. Semler (The American Ceramic Society, Westerville, OH, 1989) pp. 215–226.
19. R. H. J. HANNINK, Y. BANDO, H. TANAKA and Y. INOMATA, *J. Mater. Sci.* **23** (1988) 2093–2101 (1988).
20. K. T. FABER and A. G. EVANS, *Acta Met.* **31**(4) (1983) 565–576.
21. K. T. FABER and A. G. EVANS *ibid.* **31**(4) (1983) 577–584.
22. G. C. WEI and P. F. BECHER, *J. Amer. Ceram. Soc.* **67**(8) (1984) 571–574.
23. C. H. MCMURTRY, W. D. G. BOECKER, S. G. SESHADRI, J. S. ZANGHI and J. E. GRANIER, *Amer. Ceram Soc. Bull.* **66**(2) (1987) 325–329.
24. P. F. BECHER, C. H. HSUEH, P. ANGELINI and T. N. TIEGS, *J. Amer. Ceram. Soc.* **71**(12) (1988) 1050–1061.
25. P. F. BECHER, *ibid.* **74**(2) (1991) 255–269.
26. C. H. HSUEH, P. F. BECHER and P. ANGELINI, *ibid.* **71**(11) (1988) 929–933.
27. Z. LI and R. C. BRADT, *ibid.* **72**(1) (1989) 70–77.
28. F. F. LANGE, *J. Mater. Sci.* **10** (1975) 314-320.
29. Y. TAJIMA and W. D. KINGERY, *ibid.* **17**(8) (1982) 2289–2297.
30. A. G. EVANS, *J. Amer. Ceram. Soc.* **65**(10) (1982) 497–501.
31. Y. FU and A. G. EVANS, *Acta Met.* **30**(8) (1982) 1619–1625.
32. P. F. BECHER, *J. Amer. Ceram. Soc.* **74**(2) (1991) 255–269.
33. Z. LI and R. C. BRADT, in "Ceramic Transactions," Vol. 2, Silicon Carbide '87. edited by J. D. Cawley and C. E. Semler (The American Ceramic Society, Westerville, OH, 1989) pp. 313–339.

Received 1 October 1997
and accepted 27 April 1999